Computational Fluid Dynamics Simulations of TOPFLOW-Pressurized Thermal Shock

Yonghwy Kim [a*], Sagar Deshpande [b], Bojan Niceno [b]
[a]*FNC Technology Co., Ltd., 32F, 13, Heungdeok 1-ro, Giheung-gu, Yongin, Korea*
[b]*Paul Scherrer Institut, 5232 Villigen, Switzerland*
[*]*Corresponding author: yonghwy.kim@fnctech.com*

1. Introduction

The occurrence of Pressurized Thermal Shock (PTS) is one of the most important issues for the integrity of the Reactor Pressure Vessel (RPV) regarding the reactor lifetime safety. Pressurized thermal shock is the occurrence of sudden temperature changes on the walls of RPV, which might be embrittled by the neutron flux occurring in the reactor core.. Imagining the effect of cold water being poured in a cold glass is a vivid demonstration of a Thermal Shock. In case of the RPV, the thermal shock is accompanied by the pressure in the vessel. This phenomenon is caused by insufficient mixing of the injected cold Emergency Core Cooling (ECC) water and the hot water in the Cold Leg (CL) and the Down-Comer (DC) during the Loss Of Coolant Accident (LOCA) scenario [1].

During the PTS transients, the insufficient mixing is one of the main concerns for the two-phase configurations in a partially uncovered CL with injecting cold ECC water into the steam flow and hot primary coolant. In order to investigate mixing and heat transfer between cold and hot streams in the CL, various experimental and CFD simulation studies have been conducted in last couple of decades. A detailed review can be found in the recent literature [2]-[7]. In one of the experimental efforts, Transient twO Phase FLOW-PTS (TOPFLOW-PTS) program was conducted in the Helmholtz Zentrum Dresden-Rossendorf (HZDR) in Germany to obtain data of the two-phase configurations in air-water case without mass transfer and steam-water case with mass transfer due to condensation in the CL [8], [9].

In the test section of TOPFLOW-PTS, water is injected into the air or steam flows in a partially uncovered CL to investigate the effect of steam condensation and to examine the flow dynamics. The PTS thermal fluid dynamic phenomena are strongly influenced by the interfacial structure and turbulence: mostly interfacial momentum and heat transfer, heat transfer to walls, and to lesser extent bubble entrainment and mixing. These physical phenomena in the test section occur in the three areas: the impinging jet area, the CL stratified area, and the DC area [10].

In relation to TOPFLOW-PTS, the applicability of CFD models of the PTS were assessed within the European project Nuclear Reactor Integrated Simulation Project (NURISP) and concluded that CFD models are required to be improved for accurate predictions [5], [10]. From a couple of the previous studies based on multiphase and Reynolds Averaged Navier-Stokes (RANS) models for thermal mixing and heat transfer in the geometry of the TOPFLOW-PTS [2], [3], the local temperature distributions showed oscillatory behavior on the local monitor point close to the interface at upstream of the ECC injection. For that reason, a higher mesh resolution close to the interface and the ECC injection was proposed to improve the stability of the interface and turbulence models as well as to improve accuracy of the results [3].

To bridge the missing links, previous mesh (base grid) is refined selectively at the gas-liquid (GL) interface in two levels and in the high turbulence regions in the present study. Using the refined grids, the steady state simulations are performed in air-water case for the geometry of TOPFLOW-PTS with using VOF model to investigate the effect of mesh resolution. The assessment involves comparison of local temperature predictions, contours plots at various cut-sections and wall surface temperatures. The impact of refinement in the Pump Simulator (PS) and the ECC injection region is also evaluated. Finally, sensitivity study of two turbulence models, SST model and $k - \varepsilon$ model is also undertaken on the refined grid to verify their relative performance and stability.

2. Computational Fluid Dynamics Simulations

2.1 Geometry and Computational Grid

The TOPFLOW-PTS experiment is an integral-type, instrumented with state measuring techniques, based on the EDF 900 MWe CPY Pressurized Water Reactor (PWR) to a scale of 1:2.5 operated in France [2], [10]. The test section is composed of the CL, DC, and PS as shown in Fig. 1, together with an illustration of a real RPV which shows what TOPFLOW-PTS simulates. The CL section is simplified to a straight horizontal pipe with the ECC water injection pipe on the middle and connected with the PS and the DC at both ends.

The DC section is a simplified in the form of a flat wall to get rid of the curvature from the original RPV wall part to fit into the driving tank and connected to the downstream end of the CL pipe and the condenser unit.

The PS is a vessel that has the slightly inclined distribution plate inside and connected to the upstream end of the CL [8].

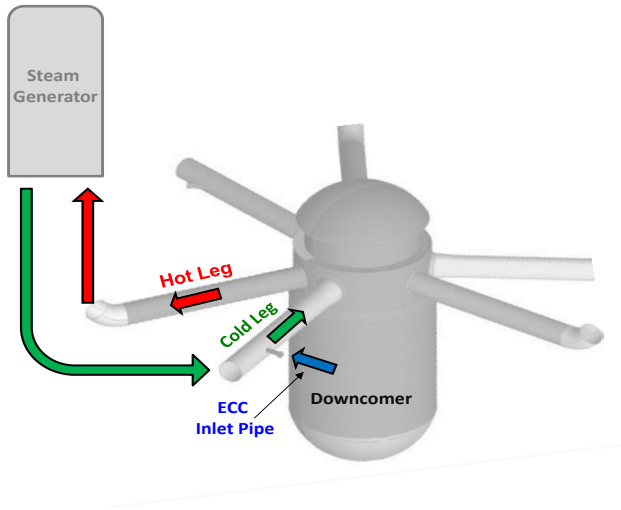

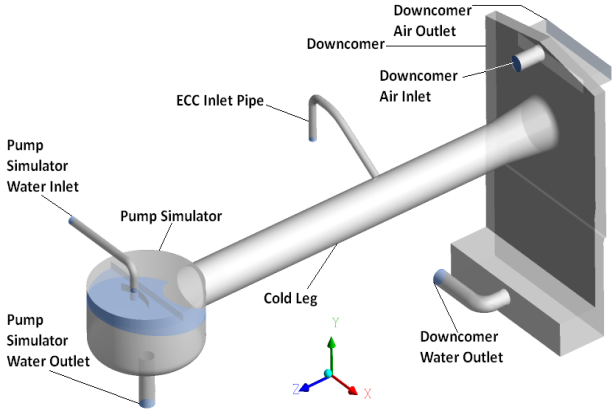

Fig. 1 Cold leg in the RPV: (top) real installation, (bottom) modeled with TOPFLOW-PTS rig.

The test rig is equipped with the measuring in-fluid Thermo-Couples (TC). Temperature is measured at 4 points by TCs, four long lances LA1, LA2, LA3, and LA4 measuring the vertical temperature distribution, supported on thin lances, and installed in the CL (Fig. 2). Additionally, wall temperature is measured using thermometry technique using an infrared camera. Details of instrumentation and uncertainty analysis may be found in [2].

2.2 Computational Grid Refinement

In the present study, three meshes were used in total. First mesh, hereafter mentioned as base case, has been used in the previous studies [2], [3]. The grid was generated in ICEMCFD by HZDR. The grid was generated in the non-orthogonal and multi-block structured grid with approximately 870,000 hexahedral cells through the entire computational domain and its sectional views are presented in Fig. 3.

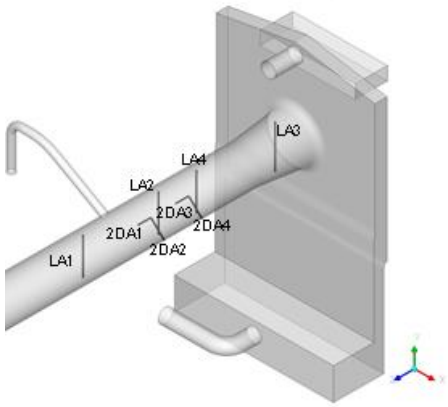

Fig. 2 Locations of TC lances in the CL of TOPFLOW-PTS

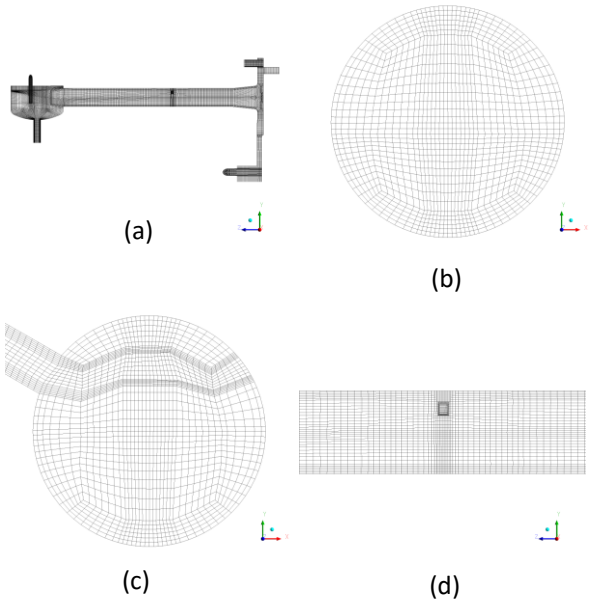

Fig. 3 Multi-block structure grids: (a) entire domain, (b) CL cross-section, (c) ECC jet injection cross-section, and (d) CL section

The other two mesh cases, of size 4.4M and 5.7M, include selective refinement (Fig. 4). A methodology of adaptive mesh refinement in FLUENT was used for local refinement with the base grid from HZDR. The first refined mesh, of size 4.4M, is obtained by refining the base grid along the GL interface horizontally (Figs. 4 b and 4 d) and in the higher turbulence regions, namely, ECC injection and PS (Fig. 4 a). The second refined mesh, of size 5.7M, includes one more level of refinement at the GL interface (Figs. 4 c and 4 e).

2.3 Boundary and Initial Conditions

Fluid properties are defined for the operating pressure

of 2.25 MPa, and boundary conditions are defined by the ratio of the PS inlet to ECC inlet mass flow rates of 1:1.7. Due to the confidentiality agreement with the TOPFLOW-PTS consortium, exact values are not specified here. The temperatures are indicated to T_{PS} for the PS inlet as the highest temperature and T_{ECC} for the ECC inlet as the lowest temperature with setting to below saturation for the operation pressure. An outlet boundary condition is set to pressure outlet at the bottom of the DC. The domain was initialized based on experimental boundary conditions. The water level was set to be constant at 50% in the CL during the simulation. Velocity and temperature were initialized at zero and perfectly mixed temperature T_{mix}, $(1.7T_{ECC} + T_{PS})/2.7$, respectively. Due to unavailability of data, the opening at the top of the DC was set as a wall.

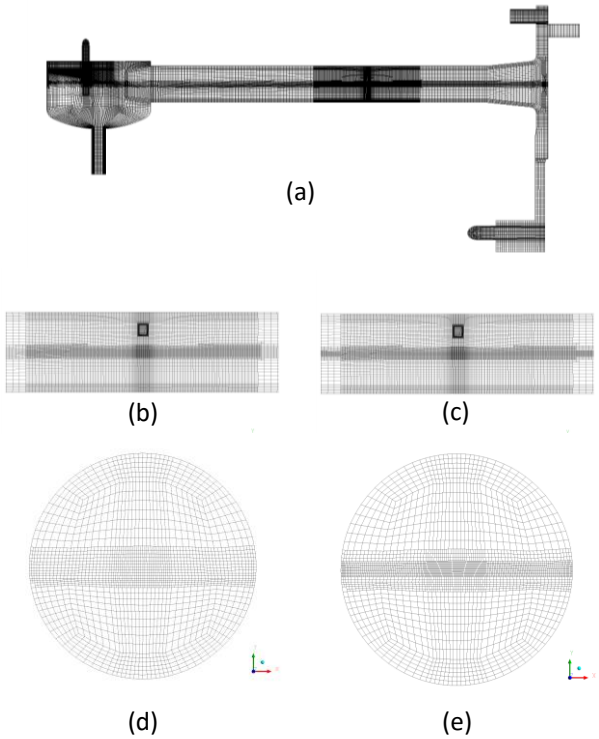

Fig. 4 Cut-sections of refined multi-block grids (a) vertical section showing refinement in the ECC and PS sections for 4.4M/5.7M cases, (b) ECC section for 4.4M case, (c) ECC section for 5.7M case, (d) cross-sectional view of the CL in 4.4M case and (e) 5.7M case.

2.4 Mathematical Model

For the implementation of TOPFLOW-PTS simulations, FLUENT 14.5 has been used. In FLUENT, a solver has been set to pressure-velocity coupled scheme, and QUICK (Quadratic Upstream Interpolation for Convective Kinetics) discretization scheme has been used for momentum and energy in Navier-Stokes conservation equations. The pseudo-transient under-relaxation method is selected for faster convergence. For multiphase modeling, VOF method is selected and free-surface interface sharpening functions are incorporated [3]. Moreover, SST $k - \omega$ model is selected for turbulence modeling. In turbulence model comparison, realizable $k - \varepsilon$ model is also used with enhanced near-wall treatment to verify the validity of a selected refined grid.

3. Results and Discussions

In this section, we analyze CFD predictions performed on three meshes, namely, the base, 4.4M and 5.7M, quantitatively as well as qualitatively. The main focus of comparing these cases is to understand the impact of interface refinement on the underlying momentum and heat transfer processes. Therefore, based on quantitative and qualitative analyses, a grid showing the best agreement with the experimental data is further used to study the performance of turbulence models. Note that the TOPFLOW-PTS experimental data is not publicly available. Thus, the results are presented in a normalized form using non-dimensional coordinates η and ξ, and temperature, θ. They are defined, as follows:

The vertical direction co-ordinate in the CL, η, is represented as:

$$\eta = 0 \ldots 1 \qquad (1)$$

where, $\eta = 0$ corresponds to an empty CL, while $\eta = 1$ corresponds to a fully filled CL. Free surface is situated at $\eta = 0.5$. The horizontal stream-wise co-ordinate is normalized with respect to the ECC injection as:

$$\xi = \frac{Z_{ECC} - Z}{D_{CL}} \qquad (2)$$

Here, D_{CL} is the CL inner diameter, Z is the co-ordinate in the horizontal stream-wise direction and Z_{ECC} represents the center-line of the ECC injection. Negative ξ corresponds to a location towards the PS and positive value of ξ represents a location towards the DC. Similarly, the temperature is normalized as:

$$\theta = \frac{T - T_{ECC}}{T_{PS} - T_{ECC}}. \qquad (3)$$

In (3), T_{ECC} and T_{PS} are the temperature of the ECC injection and the temperature of the PS injection, respectively. Equation (3) represents the normalized temperature with θ_{ECC} is equal to 0 and θ_{PS} amounts to 1.

The θ profiles are compared at lances LA1, LA2 and LA3 among the available locations. The ξ values corresponding to these lances are -1, 1 and 4.08, respectively (Fig. 5). The reason for selecting these three lances is that the lances LA1 and LA2 are close to the ECC injection and therefore show the most interesting temperature distribution in the CL. On the other hand, the lance LA3 is chosen to understand the temperature distribution at the entrance of the DC.

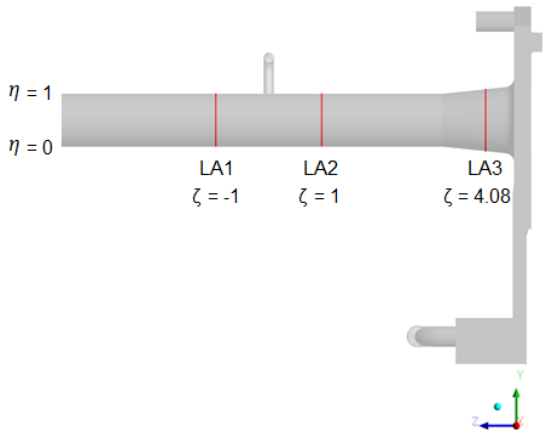

Fig. 5 Measurement locations in CL of TOPFLOW-PTS geometry

3.1 Quantitative Comparison

As a part of validation process, first step is to compare the predicted results quantitatively against the experimental thermocouple data. To eliminate local oscillatory behavior, the obtained results are averaged over the last 20,000 iterations in the steady-state simulations after residuals for continuity and energy reach below 5×10^{-6} and other variables, such as momentum, turbulence, and void fraction, reach below 10^{-4}.

The normalized temperature profiles with four different grids, the base grid, and the experiment at LA1 are shown in Fig. 6 a. In the experimental values, the temperature gradient was observed with the temperature difference, $\Delta\theta = 0.233$. The temperature distribution trend shows that the fluid temperature decreases toward the interface. This inhomogeneous distribution shows that the fluid was not mixed sufficiently at LA1. Moreover, two streams, cold ECC stream and hot CL stream, exchanged heat intensively in this region.

The predicted temperature profiles at LA1, for the base grid, are comparable to the experiment (Fig. 6 a). However, the profile shows a slightly higher temperature gradient $\Delta\theta \approx 0.260$. The local temperature values under-predict approximately 5% towards the interface and over-predict around 7% near the bottom wall ($\eta < 0.15$) as compared to the experiment. The qualitative trend also displays a slight under-prediction in the bulk region ($0.3 < \eta < 0.45$). These predictions are found within the uncertainty limit of the experiments and as shown in the previous study by Deshpande, et al. [3], interface sharpening functions improve the predictions considerably. In this study, we evaluate stabilities of these functions on refining the mesh at the interface.

For the 4.4M grid, wherein interface is refined by one level, the predictions in the bulk region ($0.17 < \eta < 0.45$) indicate reasonable improvements and temperature profiles are found to be within approximately 3% of the experimental values (Fig. 6 a). In contrast, temperature values are slightly over-predicted near the wall and under-predicted near the interface than the experiment.

For the 5.7M grid, wherein two levels of refinement are incorporated at the interface, temperature distribution trend is captured very well as against the experimental values except near the interface ($\eta \rightarrow 0.5$) where the trend is slightly deviated from the experiment, but is close to the base grid (Fig. 6 a). The temperature predictions are found to be within 2% of experimental values in the entire bulk region ($0.15 < \eta < 0.45$) as well as close to the bottom wall ($\eta < 0.15$). The temperature profile also captures a fractional dip in the temperature values in the near wall region as against the previous two mesh cases.

The temperature profiles are compared at other two locations, namely, LA2 and LA3. At the lance LA2, a key observation from the TC data specifies that two streams mix intensely in the region close to the ECC and temperature is already reaching a mixture temperature downstream in the CL at $\xi = 1.0$. The θ profiles obtained by all the meshes are very close to each other and show good agreement with the experimental data (Fig 6 b). However, a slight over-prediction is seen for all mesh cases. For example, the base grid is found to deviate around 4% in the bulk region, while profiles over-predict more than 6% near the interface as well as towards the bottom wall. The refined cases, 4.4M and 5.7M, display very close agreement in the near wall region (within 2%) and overall profile also follow the experimental values within 3% accuracy. The deviation increases closer to the interface, *i.e.*, for $\eta > 0.4$, as compared to the mean experimental θ values (Fig 6 b).

At lance LA3, θ values obtained by all the approaches predict the experimental data accurately (Fig. 4 c). The θ trend emphasizes that cold and hot streams are completely mixed at this CL location ($\xi = 4.08$) before entering the DC. At positions close to the interface ($\eta > 0.46$), all the approaches show large discrepancy against the experimental values. More importantly, the TC measurements capture significantly lower temperature readings at the interface, even crossing the limits of prescribed boundary conditions ($\theta < 0$).

There could be multiple reasons responsible for these readings. Firstly, surface waves of the liquid streams cause the thermocouple to get exposed to the air phase intermittently. As a result, wet thermocouple measures lower values due to the evaporation effects. Secondly, boundary conditions in the air phase are not exactly

measured. Also, air phase boundary conditions are not modelled exactly due to lack of available data in these locations. Further, the recirculation of air and corresponding humidity are not measured and these factors are not considered in the simulations. As far as simulations are concerned, these heat and mass transfer phenomena due to liquid evaporation and humidity effects in the air phase are not accounted for.

To summarize, quantitative analysis shows that the grid refinement at the interface and in the high turbulence region improves the prediction considerably. Ironically, at the interface all the mesh cases show identical predictions reflecting a need for improvements in the interface modeling strategies in SST based RANS approach. To understand the underlying momentum and heat transfer processes, next sections illustrate variations in velocity and temperature contours, at various cut-sections in the bulk as well as on the wall surface, due to mesh refinement.

3.2 Qualitative Bulk Profile Comparison

From the previous section, it is observed that one level mesh refinement at the interface, the temperature profiles improve in the bulk. And with the second level mesh refinement, temperature profiles improved in the near wall region in addition to the bulk region. Thus, mesh refinement certainly making positive effect on underlying mechanism that needs to be explored. The deviations in the profile can be because of better interaction of streams as well as ECC stream impingement at the interface. The streamlines presented in Fig. 7 indicate intense mixing regions close to the ECC injection ($-1 < \xi < 1$) as well as near PS injection ($-5 < \xi < -4$). On the contrary, flow in the regions between PS and ECC, *i.e.*, $-4 < \xi < -2$ as well as between the ECC and DC are streamlined (Fig. 7).

To find out the reasons, we compare the contours of velocity and turbulence kinetic energy temperature at various cut-sections. Firstly, we compare these properties on a cut-section at $\xi = -1$ (LA1). Secondly, we analyze the thermal hydraulics behavior at the ECC injection section ($\xi = 0.0$). Thirdly, we compare the fluid flow behavior close to junction of the PS ($\xi = -5.0$) and CL as well as in the middle of the PS and ECC ($\xi = -3.0$) to analyze the effect of PS on mixing process.

At $\xi = -1$, where temperature profiles are compared quantitatively in the previous section, we analyze velocity and turbulence behavior to interpret these observations. In all stream-wise velocity contours, positive superficial velocity (warm colors), represents the flow towards the PS, and the negative superficial velocity (cold colors), represents the flow in the direction of DC (Figs. 8 a – 8 c).

The relative comparison highlights lower and diffused velocity values in the top right corner for the base grid (Fig. 8 a). On the contrary, for the refined mesh cases of 4.4M and 5.7M, sharp and higher velocity region is prominent (Figs. 8 b and 8 c). These stream wise velocities in Fig. 8 verify the inverse stratified temperature profile at LA1 (Fig. 6 a). Due to the strong ECC stream flow close to the interface in this mixing zone, temperatures are lower at the interface. And high temperature PS stream mixes from the lower side of the CL resulting into higher temperatures at the bottom wall. The turbulent kinetic energy profiles also reveal significant increase in the magnitude in the regions close to the interface (Fig. 9).

In spite of having differences in the contour plots of velocity and turbulence at section $\xi = -1$, quantitative comparison highlights deviation at the interface and temperature value remaining indifferent, but improving profiles in rest of the section.. Therefore, main factor to differentiate velocity magnitudes by three grids during the fluid mixing processes is the ECC jet momentum carried in the mixing zone. For that reason, air volume fraction and water velocity contours at the ECC injection cut-section ($\xi = 0$) are investigated.

The volume fraction profiles in Fig. 10 show that for the base grid, gas-liquid (GL) interface is diffused and smeared at the ECC jet as well as at the stratified GL interface. On the other hand, 4.4M and 5.7M grids capture sharp interface profiles at the ECC cross-section. In particular, onset of interface separation occurs earlier within the ECC injection pipe for the cases of increased mesh resolution (Figs. 10 b and 10 c). Due to the early separation of liquid stream, the ECC jet width is found to be narrower compared to the base case (Fig. 10). Besides, the ECC jet impinging angle with respect to the interface was slightly higher in 4.4M and 5.7M cases compared to the base case. Thus, grid refinement in the ECC region captures mixing and heat transfer processes more effectively due to reduced numerical diffusion of momentum and energy at the interface and at the wall from the ECC jet impingement.

Variations in the ECC-jet-width predictions considerably affect the velocity distribution in the ECC jet. For example, velocity field predicted by the base case indicates a diffused and smeared patterns in the ECC jet (Fig. 11 a). In contrast, for 4.4M and 5.7M cases, the velocity fields are very similar to each other (Figs. 11 b and 11 c). In these cases of higher resolution, the maximum jet impact velocities are found to be faster at approximately $\tilde{U} \approx 1.50$ as compared to the base case where $\tilde{U} \approx 1.30$. The higher grid resolution near the interface reduces numerical diffusions of momentum and energy at the ECC jet impingement. As a consequence, less energy dissipation occurs from the impact of the ECC jet on the interface and it results in increase jet impact velocity. This faster jet impact velocity makes the momentum and energy exchange stronger after further impinging on the wall as observed

in Figs. 11 b and 11 c.

Thus, grid refinement in the ECC jet injection region influences the ECC jet behavior to be captured effectively. More importantly, changes in the momentum would affect the circulation rate in the mixing zone in the vicinity of the ECC injection resulting into better quantitative predictions, as prominently observed in the quantitative temperature profiles in the previous section (Fig. 6).

The other stream, containing hot water and coming from the PS, enters into the CL from an inclined plate in the form of a thin film. This film enters the CL at the interface. Therefore, interface predictions become important in this section as well. In this regards, the effect of changes in the flow and turbulence behavior in this section (at ξ = -5) on overall mixing process close to the ECC injection are analyzed here.

Fig. 12 presents the streamline velocity distribution at ξ = -5. The negative velocity direction in the contour represents the flow towards DC, while positive velocity direction corresponds to the flow towards PS. The results show large variations in the flow patterns between base grid and refined grids. In the case of the base grid, water film is dispersed more uniformly along the GL interface (Fig. 12 a). As a result, a vertical circulation cell is formed. On the contrary, for the cases of 4.4M and 5.7M grid, in addition to the vertical circulation cell, a stronger horizontal two loop circulation pattern is formed (Figs. 12 b and 12 c). The deviation at this cut-section is due to the liquid film formation, dispersion and flow on the PS plate.

In the case of base grid, due to the coarseness of the grid on the PS plate, diffused and thick film is predicted. Consequently, more dispersed and uniform flow is formed on the plate that enters the CL. Therefore, a dominant vertical circulation cell is formed. Two blue peaks at the interface suggest a formation of horizontal circulation cell also, however, it is of diffused nature.

In contrast, due to the refinement on the PS plate in latter two cases, liquid film is thinner, less dispersed and therefore concentrated in the central region of the PS plate (Figs. 12 b and 12 c). Because of centrally dominant flow, hot stream hits the CL interface region at higher velocity magnitudes. As a consequence, stronger two loop circulation cells are predicted in addition to the vertical circulation cells.

The turbulent kinetic energy patterns show consistency with respect to the velocity pattern in each of the cases (Figs. 13 a – 13 c). For example, for the base grid a maximum remains slightly off-center; but only one peak is seen. For other two refined grid cases, dual peak pattern is dominant. These patterns reflect high shear regions in the predicted profiles. Moreover, finer grids verify stronger impact at the GL interface and thereby more intense mixing.

Velocity and turbulence profiles highlight large variations in the qualitative mixing patterns close to the PS section. However, due to unavailability of experimental data of liquid film thickness or velocity at this section, these findings could not be validated. Interestingly, one and two level refinement show similar pattern indicating that the film flowing on the plate is captured in the same manner. This flow pattern further suggests that film formation pattern is captured well by refinement.

Although validation of the profiles could not be performed, more important task is to assess the impact of these variations on the temperature profiles in the mixing zone close to the ECC injection and more specifically at the cut-section LA1. Therefore, velocity profiles are compared at a cut-section midway between PS and ECC, i.e., at ξ = -3. The streamline velocity patterns are found to be very smooth, unidirectional and without strong flow changes (Fig. 7). More importantly, all the three mesh cases show velocities very close to each other (Fig. 14). The temperature is uniform in the entire cross-section due to present on hot stream only and therefore not presented. Based on these observations, it can be concluded that PS has very little or no effect on the mixing and heat transfer processes in the region close to the ECC injection. In other words, the length of the CL section is sufficient enough to nullify the variations at the junction of the PS and CL.

To sum up, bulk flow profiles at various cut-sections elaborate underlying transport phenomena. These profiles further show improvements and increase in inhomogeneity by capturing the liquid film thickness and distribution. Most importantly, the difference in quantitative temperature distribution is found to be because of the interface and bulk flow predictions in the ECC jet region, while impact of irregularities in the PS side mixing zone is minimal.

3.3 Qualitative Wall Surface Temperature Comparison

From previous sections, mixing zone near the ECC injection is identified to be very dynamic and having high heat transfer between the two streams. Therefore, qualitative validation of wall surface temperature variations in this region would provide more insight into in the mesh refinement study. In this section, qualitative wall temperature distributions obtained from three meshes are compared against the thermography data.

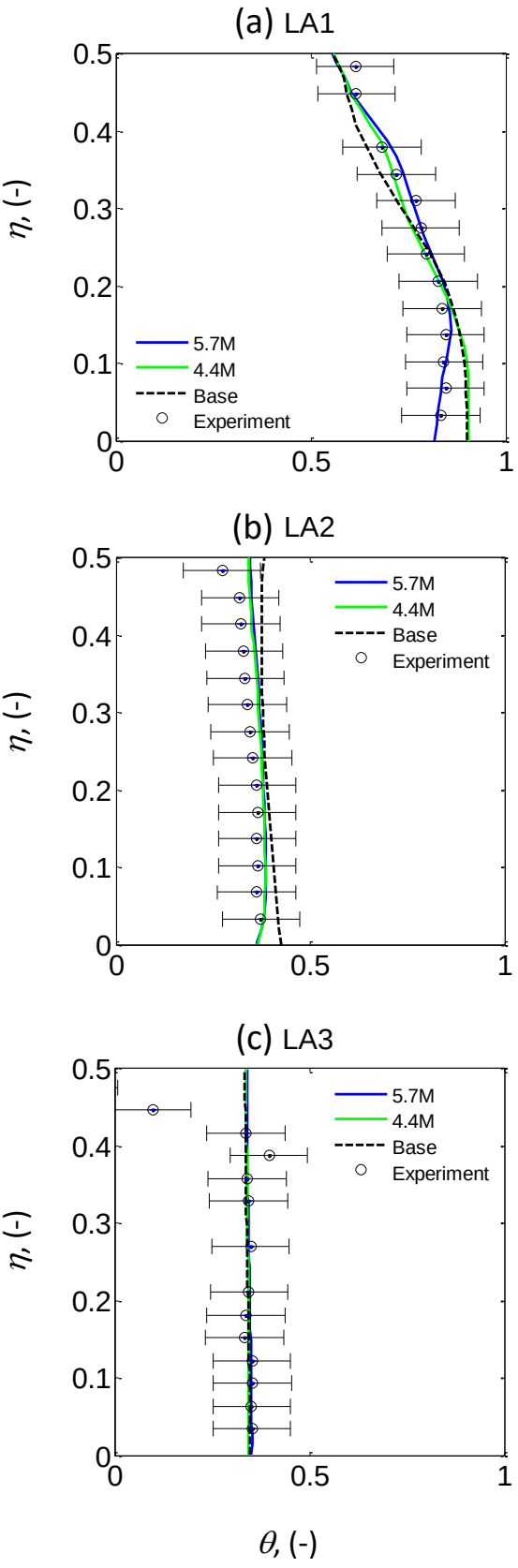

Fig. 6 Normalized temperature distribution at (a) LA1, (b) LA2, and (c) LA3 of 4.4M and 5.7M grids

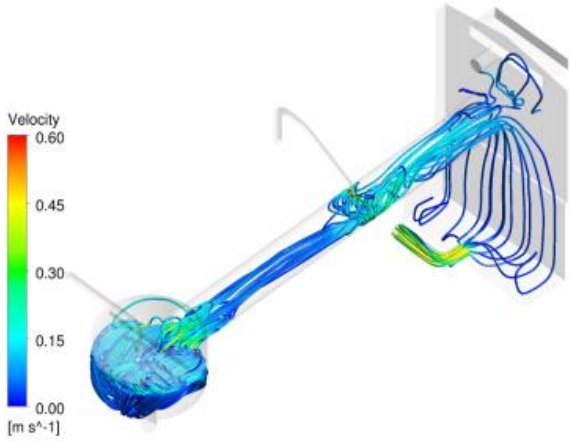

Fig. 7 Streamlines of superficial velocity in the CL

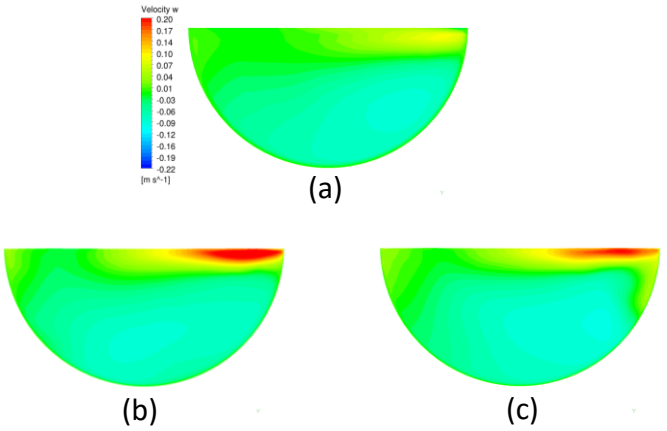

Fig. 8 Streamline water velocity at LA1 in the CL for (a) base, (b) 4.4M, and (c) 5.7M grids

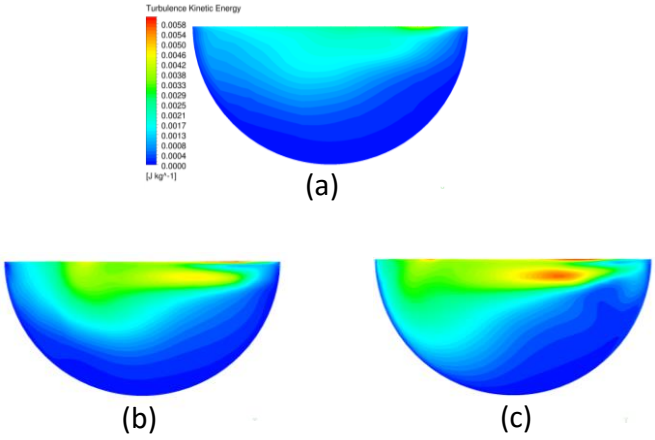

Fig. 9 Turbulent kinetic energy at LA1 in the CL for (a) base, (b) 4.4M, and (c) 5.7M grids

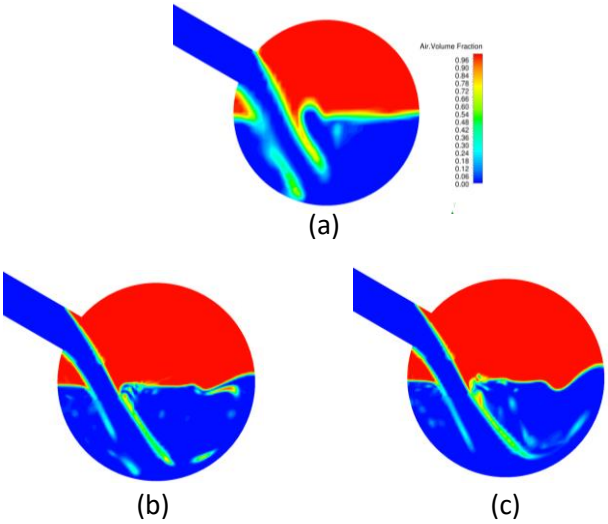

Fig. 10 Air volume fraction at the ECC jet injection cross-sections of (a) base, (b) 4.4M, and (c) 5.7M grids

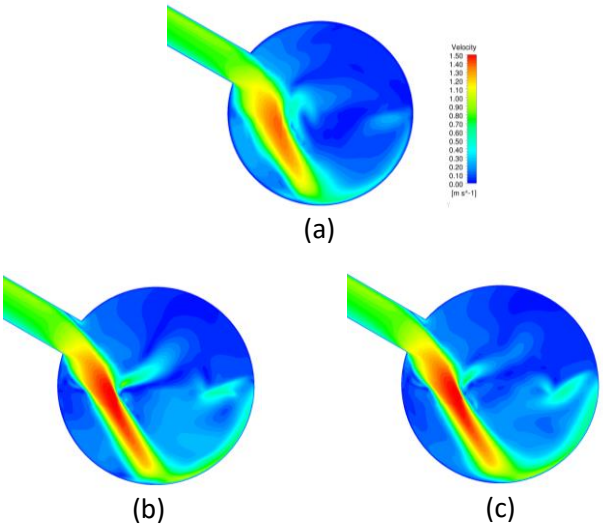

Fig. 11 Velocity field distributions at the ECC jet injection cross-sections of (a) base, (b) 4.4M, and (c) 5.7M grids

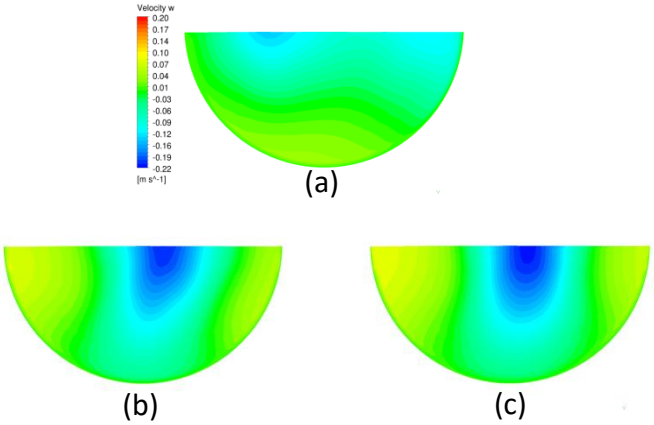

Fig. 12 Water velocity in direction *z* at ξ = -5 in the junction of the PS and the CL for (a) base, (b) 4.4M, and (c) 5.7M grids

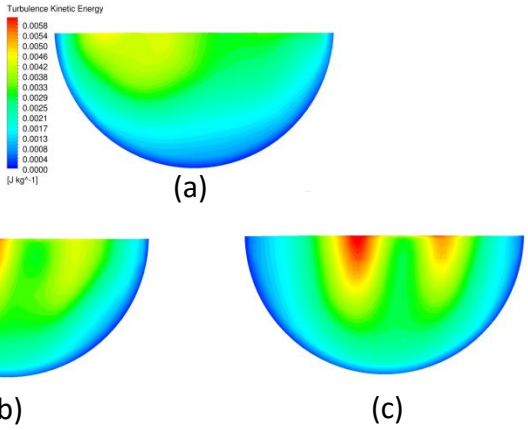

Fig. 13 Turbulent kinetic energy at ξ = -5 in the junction of the PS and the CL for (a) base, (b) 4.4M, and (c) 5.7M grids

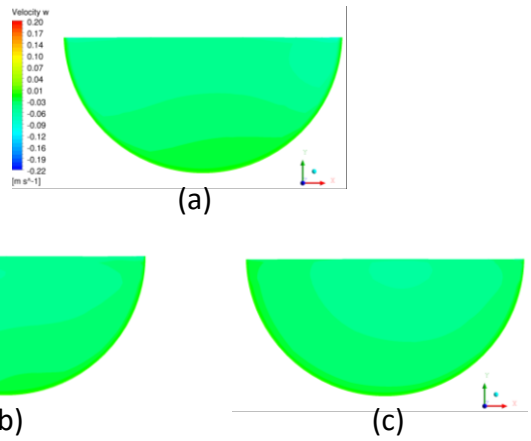

Fig. 14 Water velocities in direction z of the base grid and 5.7M grid at ξ = -3 for (a) base, (b) 4.4M, and (c) 5.7M grids

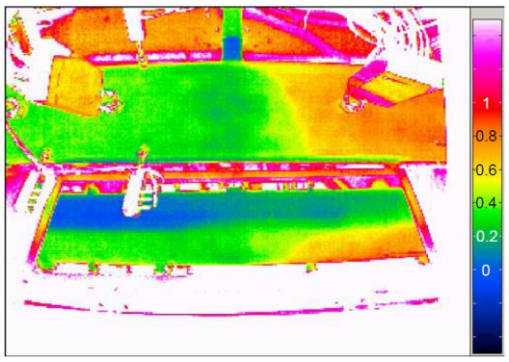

Fig. 15 Wall temperature distribution contours on the CL from the experiment in the bottom and side views

In the TOPFLOW-PTS experiments, an infrared camera was used to capture qualitative temperature distributions in the form of thermography images on the

bottom CL wall in a region close to the ECC injection [2]. The temperature distributions from the side were measured by making additional arrangements using an infrared mirror.

From the experimental wall temperature distribution, two temperature zones on the bottom wall and the side wall are apparent near the upstream of the ECC injection (Fig. 15). Between two different water temperature zones, temperature transition is observed in the form of a sharp and curved gradient line near $\xi \approx -1$. A split in the ECC jet injection behavior is also prominent. The temperature in the upstream region is equivalent to the PS injection water temperature, $\theta \rightarrow 1$. The temperature in the downstream region is quite close to the perfectly mixed temperature in the DC outlet water temperature, $\theta \rightarrow 0.37$. This observation verifies effective mixing of two streams in the CL itself as observed in all the predictions in Fig. 6 b.

To qualitatively compare the wall temperature distribution, the inner surface is selected because wall conduction is not accounted in the simulations. Additionally, the location of quantitative measurement lance LA1 is presented in Fig. 16 for reference. Although all the mesh cases capture the zone of separation quite effectively against the experimental thermography data, there are small variations in their predictions (Figs. 15 and 16). As seen from the bottom view, cold stream impaction zone on the opposite wall of the ECC injection in the base case is smaller as compared to the refined mesh cases (Figs. 16 a - 16 c). Also, the spot is tilted more towards the DC (Fig. 16 a). In contrast, 4.4M and 5.7M mesh cases reflect a broader spread toward both DC and PS (Figs. 16 b and 16 c). As a result, distribution of momentum in the upstream direction is expected to be higher in the refined meshes.

Most important aspect is the high temperature gradient region dividing hot and cold streams. In the case of base grid, this gradient is very sharp and bit straightened compared to experimental observations (Fig. 16 a). On the other hand, temperature gradient region is more dispersed and with more curved line experiments in the case of 4.4M and 5.7M meshes (Figs. 16 b and 16 c). Although qualitative temperature predictions of both these meshes look similar, a close assessment at the location $\xi = -1$ (lance LA1) marks the difference. The gradient line in the case of 4.4M grid is deviated slightly towards the DC and therefore higher temperature is seen compared to the 5.7M grid. (Figs. 16 b and 16 c).

The side view also shows qualitatively similar profiles by all the three meshes (Figs. 15 b, 16 d - 16 f). Although gas side walls are found to be relatively cooler in the side view, gas side temperatures also identify a qualitative trend similar to experimental observations. The differences can be justified due to lack of gas side boundary conditions. From the perspective of the PTS studies, the excellent bottom wall temperature predictions by CFD simulations are encouraging to extend the study to the full scale of the RPV.

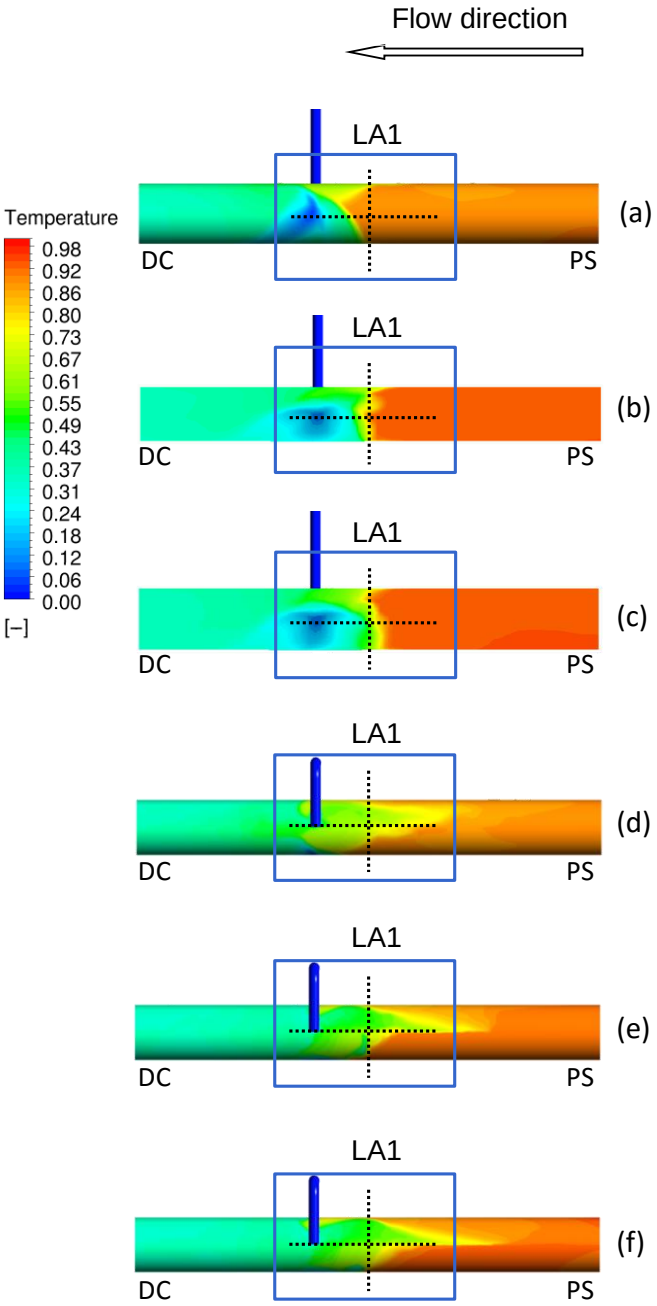

Fig. 16 Wall temperature distribution contours on the CL for three mesh cases; (a) bottom view for base grid, (b) side view for base grid, (c) bottom view of 4.4M grid, (d) side view of 4.4M grid, (e) bottom view of 5.7M grid (f) side view of 5.7M grid

From the above analysis, one can conclude that wall surface temperature contours are very sensitive in the region of ECC mixing zone. Also, interface refinements

affect the mixing and heat transfer processes significantly. Although the variations are not very high, accuracy of transport processes is important when additional phenomena of phase change are incorporated on top of the current set of modeling.

3.4 Turbulence Models

From previous sections, it is observed that the mesh with 5.7M grid shows very good agreement with experiments, qualitatively as well as quantitatively. As a next step, to check the effect of turbulence modeling approaches, two different turbulence models, SST $k-\omega$ and $k-\varepsilon$, are compared for the 5.7M grid. As seen from the Fig. 6, lance LA1 shows larger temperature distribution and this plane is very sensitive to small changes in the models. Therefore, we quantitatively compare these two turbulence models at LA1.

Fig. 17 represents performance of two turbulence models to predict the temperature distribution at LA1 (ξ = -1). Both turbulence models show very good agreement with the base grid and the experiment within 5 % accuracy. To analyze more closely, SST $k-\omega$ model predicts the temperature distribution very accurately compared to the experimental data in the near wall region. This accuracy in the near wall region can be explained by relatively stable and efficient on the energy exchange process inherent in the $k-\omega$ equations of the SST $k-\omega$ model. Moreover, $k-\varepsilon$ model shows a slight deviation of 5 % in the near wall region and the temperature distribution is converged towards the base grid predictions. This trend indicates need for wall resolution while using $k-\varepsilon$ model.

Contrast to the near wall region, the $k-\varepsilon$ model predicted the experimental values very well, within 2 %, close to the GL interface. And SST $k-\omega$ model deviates up to 5 %. The comparison of three different mesh sizes in the previous section displays similar deviation close to the interface indicating that SST model parameters need fine tuning at the free surface boundary conditions.

In the bulk region, both models predict very accurately with a slight advantage for the SST $k-\omega$ model. Interestingly, the SST model reduces to $k-\varepsilon$ in the bulk. Therefore, the under-prediction of temperature profiles is attributed to the near wall ECC water movement in the mixing zone ECC injection. Additional effect would also be due to different energy dissipation, ε, at the interface from the ECC jet impingement. These observations are found to be consistent with the literature [3].

From quantitative temperature comparison at LA1, maximum deviation in two turbulence models is found near the bottom wall (Fig. 17). Although the difference in temperature predictions is less than 7%, wall surface temperature contours may highlight performance of turbulence models in the near wall region. To get more insight into each of the turbulence models and after learning from the previous sections, we first analyze the velocity and void fraction distribution on the cut-section at the center of the ECC injection (ζ = 0.0). Further, wall surface temperature is compared in the bottom view of the CL.

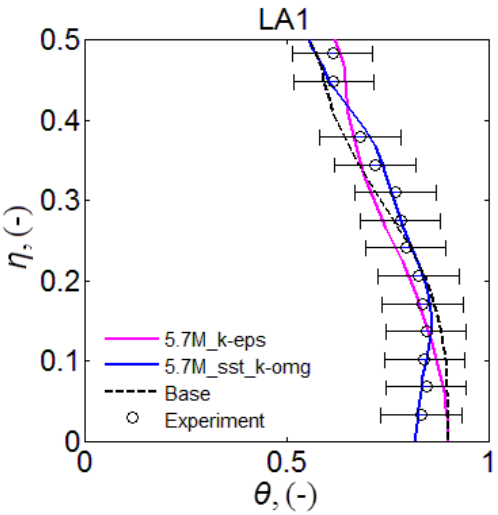

Fig. 17 Temperature distribution profile at LA1 for the SST $k-\omega$ and k–ε models

From the contour plots of air volume fraction and velocity in Figs. 18 and 19, respectively, two turbulence models are compared. There are many identical features observed in the comparison that emphasize the independence of turbulence models. To elaborate, firstly, the ECC jet separation occurs at same location inside the ECC injection pipe (Fig. 18). Secondly, jet width is same in both the cases. Further, jet velocities are found to be identical as well (Fig. 19). These similarities in the predicted profiles show that the transport phenomena in the ECC injection is governed by the jet motion in the air, interface, and in the liquid phase. By the working principle, both turbulence models inherently use k-ε model in the bulk. Main difference could exist at the GL interface where momentum is exchanged across the interface and interface boundary conditions vary in both these models. Interestingly, both the models show very good agreement in this jet region. These observations prove that in the SST model, smooth transition between k-ε and k-ω equations using blending function is modeled very accurately in the presence of strong jet impingement phenomenon.

A small difference in the velocity profiles begins to develop in the liquid phase as it approaches the front wall. The jet entrainment region in the SST model is slightly more dispersed. More importantly, as the flow moves along the CL pipe surface, differences become

more visible in the dispersed jet motion along the wall and circulation cells in the ECC cut section show a slim deviation. The momentum in the SST model is slightly higher compared to the k-ε model and may vary near wall temperature profiles.

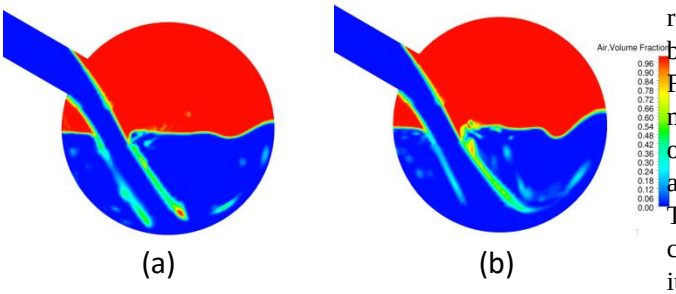

Fig. 18 Air volume fractions at the ECC jet injection cross-section of (a) $k-\varepsilon$ model and (b) SST $k-\omega$ model with 5.7M grid

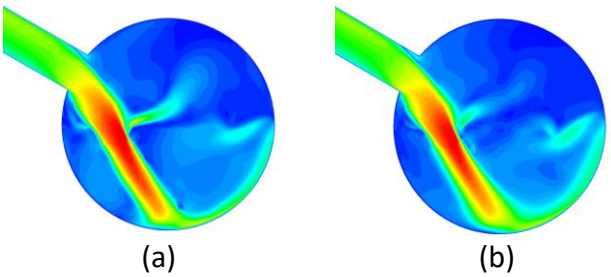

Fig. 19 Velocity field distributions at the ECC jet injection cross-section of (a) $k-\varepsilon$ model and (b) SST $k-\omega$ model with 5.7M grid

The wall surface temperature profiles are therefore important to locate differences in the near wall flow as well as boundary layer turbulence mechanisms. These wall temperature profiles would also help in understanding reasons for the differences in the temperature values at LA1. Comparison of wall surface temperature for mesh sensitivity analysis in Fig. 16 indicate that the side wall profiles are very close to each other and do not add any additional information. Moreover, they create ambiguity in the air phase which is not modeled due to lack of boundary conditions. Considering these factors, we only compare the bottom view of the wall surface temperature.

From Fig. 20, slight but important variations in the predictions of two turbulence models are seen. Firstly, the jet impaction zone in SST models is more dispersed and spread in both directions as against the k-ε model. More specifically, this behavior at impact is consistent with the jet dispersion and entrainment from the surrounding bulk region (Fig. 19).

The high temperature gradient region between hot and cold streams is captured very well using both the models (Fig. 20). The detailed comparison of contour plots at the location lance LA1 points out that this thermal demarcation line is shifted marginally towards the ECC side in the case of k-ε model. As a result, k-ε model predicts higher temperature in the near wall region in Fig. 17 as well.

On the contrary, SST model identifies a dip, which is visible from the wall temperature profiles also. The reason for this deviation lies in the ECC stream flow behavior in the near wall region past impingement. From Fig. 20, in the SST model, cold spot clearly shows more momentum transferred toward PS. Therefore, overall gradient is shifted towards the PS resulting into a dip in temperature in the near wall region in Fig. 17. Thus, it can be concluded that near wall predictions are considerably improved in the SST model and it remains its key strength in two phase simulations also provided interface transfer in the jet region is captured correctly.

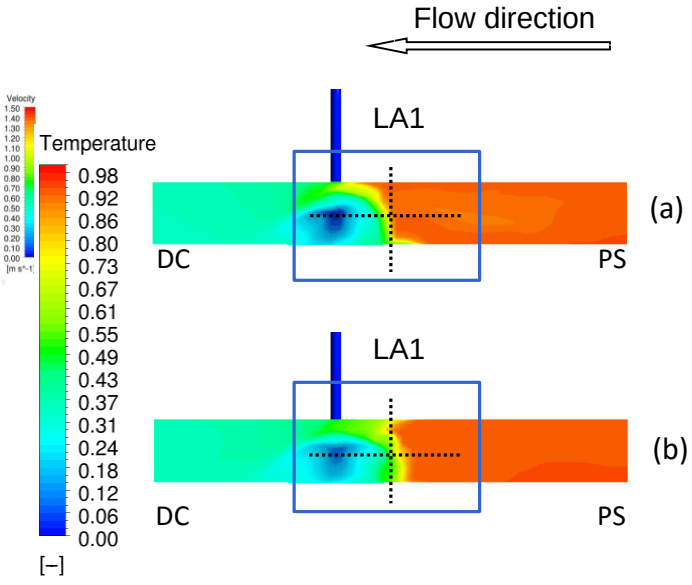

Fig. 20 Averaged CL wall temperature distributions with 5.7M grid from (a) bottom view of $k-\varepsilon$ model and (b) side view and (c) bottom view of SST $k-\omega$ model and (d) side view

To sum up, the finest grid, with 5.7M cells, is validated for the both turbulence models. This validation is verified quantitatively by the normalized temperature distributions and qualitatively by the averaged wall temperature distribution for both turbulence models. Consequently, the finest grid can be used for the steam-water simulation and further CFD application to a full scale RPV.

4. Conclusions

The present study comprises interface refinement and turbulence model studies as a part of validation of TOPFLOW-PTS geometry for the air-water two phase stratified flow condition. Main features of the study are as follows:

(1) Quantitative bulk temperature analysis emphasizes that all the mesh cases are within the uncertainty limit of experimental data. Moreover, there is significant improvement in the predicted local temperature values, which are predicted within 2% against the experimental values.

(2) From qualitative bulk flow contours, it can be concluded that the variations in the ECC jet region has most significant effect on the mixing and heat transfer process. On the contrary, although inhomogeneity is observed in the PS region after mesh refinement, it has insignificant effect in the mixing of hot and cold stream.

(3) Wall surface temperature distribution is found to be very sensitive to refinement and qualitative differences in the profiles are found to be prominent. After mesh refinement at the interface, jet behavior is captured more effectively and so as the mixing.

(4) The comparison two turbulence models reveal the benefit of using SST model due to the modeling advantage in the near wall region. However, at the GL interface more work is required to fine tune the bridging parameters in the SST model and k-ε model still shows upper hand in the interface region.

In conclusion, the grid refinement at the interface and in the high turbulence region improves the prediction due to improvements in the interphase momentum and heat transfer phenomena. Moreover, this method of selective mesh refinement has been verified and can be very useful for the transient PTS studies of full scale models where in liquid level changes in the cold leg from fully filled to empty scenario. Also, this method would be handy to implement gradient dependent phase change models effectively.

REFERENCES

[1] S. M. Willemsen and E. M. J. Komen, "Assessment of RANS CFD Modelling for Pressurised Thermal Shock Analysis," presented at the The 11th International Topical Meeting on Nuclear Thermal-Hydraulics (NURETH-11), Popes' Palace Conference Center, Avignon, France, 2005.

[2] P. Apanasevich, P. Coste, B. Ničeno, C. Heib, and D. Lucas, "Comparison of CFD simulations on two-phase Pressurized Thermal Shock scenarios," *Nuclear Engineering and Design*, vol. 266, pp. 112-118, January 2014 2014.

[3] S. S. Deshpande, B. Niceno, A. Mutz, and J. Klügel, "Multiphase and Turbulence Model's Sensitivity Study in Pressurized Thermal Shock Simulations of the TOPFLOW Experiment," in *International Congress on Advances in Nuclear Power Plants (ICAPP)*, Charlotte, USA, 2014, p. 10.

[4] D. Lucas, D. Bestion, P. Coste, J. Pouvreau, C. Morel, A. Martin, *et al.*, "Main results of the European project NURESIM on the CFD-modelling of two-phase Pressurized Thermal Shock (PTS)," *Kerntechnik : independent journal for nuclear engineering, energy systems, radiation and radiological protection*, vol. 74, p. 5, November 2009 2009.

[5] D. Bestion, "Extension of CFD Codes Application to Two-Phase Flow Safety Problems," *Nuclear Engineering and Technology*, vol. 42, pp. 365-376, August, 2010 2010.

[6] T. Seidel, M. Beyer, U. Hampel, and D. Lucas, "TOPFLOW-PTS air-water experiments on the stratification in the ECC nozzle and the ECC water mixing during PTS scenarios," presented at the The 14th International Topical Meeting on Nuclear Reactor Thermal Hydraulics (NURETH-14), Toronto, Ontario, Canada, 2011.

[7] P. Apanasevich, D. Lucas, and T. Höhne "Numerical simulations of the TOPFLOW-PTS steam-water experiment," presented at the The 14th International Topical Meeting on Nuclear Reactor Thermal Hydraulics (NURETH-14), Toronto, Ontario, Canada, 2011.

[8] P. Péturaud, U. Hampel, A. Barbier, J. Dreier, F. Dubois, E. Hervieu, *et al.*, "General Overview of the TOPFLOW-PTS Experimental Program," presented at the The 14th International Topical Meeting on Nuclear Reactor Thermal Hydraulics (NURETH-14), Toronto, Ontario, Canada, 2011.

[9] P. Apanasevich, D. Bestion, P. Coste, C. Raynaud, C. Heib, M. Scheuerer, *et al.*, "Synthesis and Conclusions on PTS Modelling," NUclear Reactor Integrated Simulation Project (NURISP), 7th Framework Programme EURATOM, Project Report30 January, 2012 2012.

[10] D. Lucas, D. Bestion, E. Bodèle, P. Coste, M. Scheuerer, F. D'Auria, *et al.*, "An Overview of the Pressurized Thermal Shock Issue in the Context of the NURESIM Project," *Science and Technology of Nuclear Installations*, vol. 2009, 21 February 2008.